

HST/NICMOS Observations of Fast Infrared Flickering in the Microquasar GRS 1915+105

Stephen S. Eikenberry¹, Shannon G. Patel¹, David M. Rothstein², Ronald Remillard³, Guy
G. Pooley⁴, Edward H. Morgan³

ABSTRACT

We report infrared observations of the microquasar GRS 1915+105 using the NICMOS instrument of the Hubble Space Telescope during 9 visits in April-June 2003. During epochs of high X-ray/radio activity near the beginning and end of this period, we find that the $1.87\mu\text{m}$ infrared flux is generally low (~ 2 mJy) and relatively steady. However, during the X-ray/radio “plateau” state between these epochs, we find that the infrared flux is significantly higher ($\sim 4 - 6$ mJy), and strongly variable. In particular, we find events with amplitudes $\sim 20 - 30\%$ occurring on timescales of $\sim 10 - 20$ s (e-folding timescales of ~ 30 s). These flickering timescales are several times faster than any previously-observed infrared variability in GRS 1915+105 and the IR variations exceed corresponding X-ray variations at the same (~ 8 s) timescale. These results suggest an entirely new type of infrared variability from this object. Based on the properties of this flickering, we conclude that it arises in the plateau-state jet outflow itself, at a distance < 2.5 AU from the accretion disk. We discuss the implications of this work and the potential of further flickering observations for understanding jet formation around black holes.

Subject headings: accretion, accretion disks — black hole physics — infrared: stars — stars: individual (GRS 1915+105) — X-rays: binaries

1. Introduction

As the archetypal microquasar, GRS 1915+105 offers great promise as the potential key for understanding the formation of relativistic jets in black hole systems. GRS 1915+105 was

¹Department of Astronomy, University of Florida, Gainesville, FL 32611

²Department of Astronomy, Cornell University, Ithaca, NY 14853

³Department of Physics, Massachusetts Institute of Technology, Cambridge, MA 02138

⁴Cavendish Laboratory, Cambridge University

first discovered as a hard X-ray transient (Castro-Tirado et al. 1994), and then later seen as the first-known superluminal jet source in the Galaxy (Mirabel & Rodríguez 1994). Further study revealed a rich variety of X-ray, infrared (IR), and radio variability from this system (see Mirabel & Rodríguez (1999) and references therein). Among these, Fender et al., (1997) discovered radio and infrared flaring on the same day (in disjoint observations), each displaying a ~ 30 -minute quasi-periodicity. Later simultaneous observations in the X-ray/IR and X-ray/IR/radio showed that these events tied together activity in the inner accretion disk (seen in the X-ray) with synchrotron jet ejections (seen in the IR and radio) (Eikenberry, et al. (1998a); Mirabel, et al. (1998); Fender & Pooley, (1998)). Thus, GRS 1915+105 seemed to be living up to its potential as a prototype source for investigations of the disk-jet connection in black hole binaries.

Since then, continued study has revealed that the disk-jet connection in GRS 1915+105 takes multiple, apparently distinct, forms. Eikenberry, et al. (2000) describe three types of long-wavelength variability: large-amplitude superluminal radio events (Class A); the ~ 30 -minute IR/radio oscillations noted above associated with hard X-ray dips (Class B); other IR/radio flares associated with individual soft X-ray oscillations (Eikenberry, et al. (2000); Rothstein, et al. (2005)) (Class C). The Class B and C events share similar radio properties (e.g. Klein-Wolt et al. (2002)), but the Class B IR flares are significantly brighter ($\sim 200 - 300$ mJy) than their class C counterparts ($\sim 5 - 10$ mJy), and the X-ray properties of these differ (Rothstein, et al. (2005); Mikles, et al. (2006)). Both of the observed IR event types have e-folding rise times of $\sim 200 - 300$ s.

To date, no IR counterparts to Class A events have been reported, though there is some evidence for extended IR jet emission (Sams, et al. (1996); Eikenberry & Fazio (1997)). This has been due in part to the transient nature of these events, with occurrence rates of only one every few years since 1994. However, detailed study has revealed an apparent pattern in these events which could allow the prediction of Class A events with lead times of a few weeks. Occasionally, GRS 1915+105 enters a “plateau state” (Foster et al., (1996); Fender, et al. (1999)), where the X-ray count rates are relatively low, dominated by a hard power-law component, and with strong quasi-periodic oscillations at frequencies $\sim 1 - 10$ Hz. The radio emission from GRS1915+105 is generally elevated and quasi-steady ($\sim 50 - 200$ mJy). It seems that the beginning and end of these plateaux are marked by large-amplitude radio flares (Klein-Wolt et al. 2002), and that just before they post-plateau flare the X-ray hardness ratio begins curving towards softer values over $\sim 10 - 20$ days. By identifying plateaux via X-ray and radio monitoring observations, we can thus hope to schedule ground- and space-based telescope resources catch the IR behavior of GRS 1915+105 during these events. With this goal in mind, we proposed Target of Opportunity (TOO) observations of GRS 1915+105 using the Near-Infrared Camera and Multi-Object Spectrograph (NICMOS)

instrument (Thompson, et al. 1998) on the Hubble Space Telescope (HST), triggered by X-ray/radio observations of a plateau state nearing its end, as observed by the All-Sky Monitor (ASM) of the Rossi X-ray Timing Explorer (RXTE) and the Ryle Telescope.

In the sections below, we first describe the observations taken as part of this program, and the data reduction techniques used to analyze them. We next describe the results of these analyses, including the identification of fast IR flickering from GRS 1915+105 during the plateau state. We then move on to discussion of the implications of these observations for understanding the formation of jets in GRS 1915+105. Finally, we present the conclusions based on these results.

2. Observations and Data Analysis

2.1. Infrared Observations

The NICMOS observations we report here were taken as TOO data with HST. We triggered the TOO on MJD 52732 (3 April 2003), based on the combination of a “plateau” state in GRS 1915+105 lasting > 10 days, and the beginning of a curving drop in the HR2 hardness ratio in data from the RXTE ASM. We then observed GRS 1915+105 using NICMOS over the span of nine visits from 2003 April 7 to 2003 June 24 (see Table 1). For each visit, we used the F187W filter ($1.75 - 2.0\mu\text{m}$) with the NIC2 detector (256×256 -pixel HgCdTe array, $19.2'' \times 19.2''$ field of view) for imaging observations and the F240M ($2.3 - 2.5\mu\text{m}$) and G206 ($1.4 - 2.5\mu\text{m}$) direct-grism filter pair with NIC3 (256×256 -pixel HgCdTe array) for spectroscopic observations. We also made polarimetric observations with the long-wavelength polarizers ($1.9 - 2.1\mu\text{m}$) and NIC2. All exposures were set to MULTIACCUM mode, with multiple non-destructive reads allowing us to analyze the behavior of the source on time scales shorter than the total exposure times. For each of the first three visits, we obtained a set of 5 dithered 72-s images using the F187W filter, and a set of 12 dithered 56-s polarized images (4 in each of 3 polarization angles: 0° , 120° , 240°).

We processed data taken with the F187W and polarization (POL) filters through the standard NICMOS calibration pipeline, CALNICA. We also processed the grism data with CALNICA, with the exception of the flatfield correction, which was determined upon extraction of individual spectra through CALNICC. We further processed and combined all dithered images with CALNICB.

For each F187W MULTIACCUM frame, we carried out photometry for GRS 1915+105 and for a nearby comparison star (Star A – see e.g. (Eikenberry, et al. 1998a)) in the same field of view. We defined an aperture with a 6 pixel radius ($\sim 0.5''$) around each star,

which just encompassed the first diffraction ring, and subtracted the background flux from an annulus with inner radius of 15 pixels ($\sim 1.1''$) and outer radius of 18 pixels ($\sim 1.4''$) to calculate the flux. We found typical background count rates for the F187W filter of ~ 0.15 DN/s. We replaced any isolated bad pixels within the photometric aperture with the median of the adjacent pixels. We omitted results for a star in a given readout if groups of bad pixels were located within its aperture. We calculated the uncertainty in background-subtracted flux using the associated error array for each exposure, and then multiplied by the PHOTFNU keyword in the header to convert to units of flux density. We calculated values of flux density for MULTIACCUM exposures at NICMOS STEP8 time intervals by first extracting individual readouts from the IMA FITS file extensions, and then determining the count rates during a given interval by finding the difference in total counts between readouts and dividing by the time interval.

We also included the polarimetry data in our photometric results using the same calculation procedure as above for the F187W data. (Due to highly-variable IR emission from GRS 1915+105 during this epoch (see below) and the sequential procedure of the polarimetry measurements with NICMOS, we could not extract meaningful polarimetric measurements for the core source.) We found background count rates for the POL filters of ~ 0.23 DN/s. While differential polarization may affect absolute flux comparisons between GRS 1915+105 and Star A, it is only on the order of a few percent or less, and should not significantly impact measurements of time-variability in flux within a given filter/polarization.

2.2. Radio Observations

The Ryle Telescope has been used to monitor a small number of variable and transient sources, including GRS 1915+105, at 15 GHz (during gaps in its primary CMB-related program). The observational details are as described by Pooley & Fender (1997); typical runs are for an hour or so, with longer times for some coordinated programs. The data points shown in Fig 1 are 5-min averages, on which the noise level is about 2 mJy rms, and the overall flux-density scale has an uncertainty of about 4%.

2.3. X-Ray Observations

For X-ray observations of GRS 1915+105, we used both the All-Sky Monitor (ASM) and the Proportional Counter Array (PCA) instruments of the *Rossi X-ray Timing Explorer* (RXTE). The ASM uses scanning masked proportional counters to provide “snapshot” ob-

servations of X-ray sources distributed across the sky, with typical sampling frequencies of several measurements per day (for details on the ASM, see Levine et al. (1996)). For monitoring the X-ray behavior of GRS 1915+105 during the IR observations, we used the dwell-by-dwell count rate and hardness ratio (HR2) downloaded from the ASM web site.

The PCA instrument on RXTE uses up to 5 proportional counter units (PCU) with large collecting area for detailed pointed observations (for details on the PCA, see Jahoda et al., (2006)) . For specific pointed observations, we analyzed the light curves, energy spectra, and power density spectra of GRS 1915+105. We used the FTOOLS package for RXTE to generate light curves with time resolutions of 1-second (using the Standard1 data mode) and 0.020-seconds (using the binned 8ms data mode). For spectral analyses, we used the XSPEC package together with FTOOLS v5.2 to analyze Standard2 data (16-second time resolution and 129 energy channels over the 2-60 keV energy range). We used standard procedures for response matrix generation, background estimation and subtraction, and correction for PCA deadtime. We then used XSPEC v11.2 to fit the 2.9-25 keV spectrum with a standard model for black hole candidates consisting of a “soft” component (which peaks in the low-energy X-rays” modeled as a multi-temperature disk blackbody (e.g. Mitsuda, et al. (1984)) and a “hard component” (which extends to the higher-energy X-rays) modeled as a power law, both modified by interstellar absorption corresponding to a fixed hydrogen column density of $N_H = 6 \times 10^{22} \text{cm}^{-2}$ (Muno, et al. 1999). We added a systematic error of 1% to the spectrum before performing the fit.

3. Results

3.1. The Multi-Wavelength Context

Figure 1 shows the multi-wavelength behavior of GRS 1915+105 during the period of the Spring 2003 HST observations. The first ~ 25 days of these lightcurves show GRS 1915+105 to be in a typical “plateau” state, with low, steady, hard X-ray emission and elevated radio flux. Near MJD 52735, the X-rays reveal a sharp outburst accompanied by radio variability – the curvature in X-ray hardness ratio leading up to this caused us to trigger the HST TOO as described above, in anticipation if a plateau-ending outburst. However, rather than showing a very large outburst signalling the end of the plateau, GRS 1915+105 showed a rather modest outburst and then *returned* to the plateau state. It then continued on in this state until near MJD 52785. Then, a second outburst led to the actual termination of the plateau state.

In Table 1, we present the average IR flux densities for each visit, star and filter type

(F187W and POL). Note that the nine data points in Figure 1c indicate the mean flux density value for each visit, while the bars represent the *range* of flux density values rather than uncertainty. The light curve in Figure 2 displays the range of IR flux density for GRS 1915+105 and also presents the mean flux density of the comparison star for each visit. In Figure 2, the error bars represent the standard deviation in the measured flux of the comparison Star A over the nine visits, which also gives a reasonable estimate of the uncertainty in flux density for GRS 1915+105. These errors are significantly larger than those derived from the CALNICA pipeline error arrays, indicating some additional uncertainty in the photometry. However, when we use the CALNICA error estimates to fit a constant flux density to Star A *within* a single visit, we obtain reduced chi-squared values of ~ 1 , indicating that the CALNICA error estimates are valid within a single visit. We attribute the additional between-visits variations in the Star A photometry to possible PSF variations from the telescope and/or NICMOS instrument. We can see from Figure 2 that GRS 1915+105 is higher in both flux and fractional variability in Visits 2-4, as compared to Visit 1 and Visits 6-9. Interestingly, these visits (2-4) correspond to the time period *between* the major X-ray/radio variability episodes described above. When the X-ray flux is high/variable, the IR flux density seems suppressed and relatively steady.

3.2. Fast IR Flickering

To further illustrate the intra-visit IR variability from GRS 1915+105, we present selected segments of the light curves in Visits 2-4 in Figure 3, along with the accompanying photometry of Star A for comparison. At times, GRS 1915+105 exhibits significant ($> 20\%$ amplitude) variability from one 8-second MULTIACCUM readout to the next. We note that the visit-to-visit instability in the photometry is not an issue for these rapid fluctuations, as shown by the stability of Star A, which has similar brightness to GRS 1915+105, but is much more stable over these same timespans. As noted above, the residuals of the flux density values for Star A to a best-fit constant value have $\chi^2_\nu \sim 1$, indicating that these uncertainties are accurate within a given visit. Typical events in Figure 3 have $\sim 5 - 10\sigma$ statistical significance. Thus, we conclude that this flickering is in fact intrinsic variability in GRS 1915+105. We quantify the mean IR flux at $1.87\mu\text{m}$ and the sample RMS excess variability in that band (8 s bins) in Table 1, so that the IR flickering rates can be compared within the set of HST results and also with respect to results from other wavebands.

We characterized the timescale of these flickering events assuming an exponential rise time for IR flares. We derived characteristic e-folding timescales using adjacent MULTIACCUM readouts (Table 2), calculating the uncertainty by simple propagation of errors from

the flux density uncertainties. The upper-limit timescale column in Table 2 indicates the maximum characteristic rise time based on the highest possible flux value (within uncertainties) at the beginning of a time interval and the lowest possible flux value at the end of it. Many flickering events show best-estimate e-fold timescales of ~ 30 s, and several have firm upper limits on this number of < 40 s. We note that these timescales are nearly an order of magnitude shorter than the fastest previously-reported timescales for long-wavelength (IR/radio) variability from GRS 1915+105 (e.g. Eikenberry, et al. (1998a); Eikenberry, et al. (2000)).

3.3. X-ray Behavior Associated with the Fast IR Flickering

We have examined the X-ray spectra and power density spectra (PDS) derived from RXTE pointed observations of GRS 1915+105 obtained near the times of the HST observations (Table 1). Particularly relevant are the RXTE observations made on 5 days (2003 April 10, 16, 23, May 1 and 7) that are interleaved with HST visits 2-5. The X-ray spectral properties during this epoch of rapid IR flickering are typical of the radio plateau state, showing a power-law dominated spectrum with a photon index, $\Gamma \sim 2.1$ – 2.3 (see Muno, et al. (2001)). The PDS during these times are similar, and they are likewise typical of the plateau state. The first two of these PDS (April 16 = MJD 52745.1 and April 23 = MJD 52752.2) are shown in Fig. 4, using the full PCA bandpass, which is effectively 2–40 keV. These PDS are subtracted for deadtime-corrected Poisson noise, normalized to power density (P_ν) in units of $(rms/mean)^2 \text{ Hz}^{-1}$, and then displayed as $\log(\nu \times P_\nu)$ vs. $\log \nu$.

The PDS shows a strong QPO just below 1 Hz, along with its second harmonic. These features are superposed on a strong and extremely broad peak in the power continuum that is centered just above 1 Hz. It has been argued that the broad power peak is a specific yet unexplained X-ray signature of the steady jet in the hard state of black hole binaries (Remillard 2004). Since the X-ray PDS exhibits little change over the interval of 2003 April–May, we can investigate the X-ray and IR connection by comparing the flickering amplitudes at the 8 s timescale of the IR light curve. When the X-ray light curves are examined in 8 s bins, the sample standard deviations for each of the 5 relevant PCA observations are all in the range of 2.4–3.0 % of the mean count rate (2–40 keV). This result represents the source flickering amplitude, since the Poisson variations for these data are well below 1%. These 8 s flickering amplitudes also represent the X-ray behavior associated with the jet, since, as noted above, the X-ray spectrum is dominated by nonthermal emission that is typical of the plateau state, or more generally the X-ray hard state associated with the presence of a steady radio jet (McClintock & Remillard, 2006). One can derive the analogous 8 s

flickering amplitudes for the IR band using the results given in Table 1. The source RMS excess variability amplitude (i.e. $\sqrt{\sigma_{sample}^2 - \sigma_{meas}^2}/mean$, where σ_{meas} are the measurement errors) is in the range of 4-8 % for HST visits 2–5. This exceeds the equivalent flickering amplitude in the X-ray band by a factor of 2–3. In addition, the baseline IR flux contributed from the donor star could be in the range of ~ 2 mJy, in which case the jet flickering at 8 s would be elevated to the range of ~ 10 %

4. Discussion

4.1. The Diversity of IR Variability in GRS 1915+105

The type of rapid IR variability described above is particularly intriguing in that it seems to be unrelated to the previous types of IR variability observed in GRS 1915+105 (e.g. Rothstein, et al. (2005); Eikenberry, et al. (2000); Bandyopadhyay, et al. (1998)). First of all, this IR flickering, while small in amplitude, is significantly faster than previous IR flares, which seem to have e-folding timescales of $\sim 200 - 300$ s, as compared to the $\sim 25 - 60$ s timescales seen here. Thus, the flickering is $\sim 4 - 10$ times faster than any previously-reported IR variability from GRS 1915+105. Second, in these observations we see no apparent association between IR flickering events and any similar X-ray events. This is also in stark contrast to previous IR flares of various types in GRS 1915+105, all of which seem to be associated with significant activity in the X-ray band as revealed through relatively large-amplitude changes in the X-ray lightcurve and/or spectrum (e.g. Rothstein, et al. (2005); Eikenberry, et al. (2000); Eikenberry, et al. (1998a); Eikenberry, et al. (1998b); Mirabel, et al. (1998); Fender et al., (1997)). We note that our observations above *do* reveal significant X-ray variability on *faster* timescales than the IR flickering. However, any X-ray variability is much smaller in amplitude when smoothed to the same time resolution as the IR data. Thus, the rapid IR flickering we report here seems to be an entirely new kind of IR variability in GRS 1915+105.

4.2. IR Emission and Relativistic Jets in the Plateau State

As shown above (Figures 1-2), the IR flux density and fractional variability from GRS 1915+105 are significantly enhanced during the plateau state, even though the X-ray flux is lowest and steadiest during this time period. A number of observations indicate that during such plateaux, GRS 1915+105 exhibits a quasi-continuous radio synchrotron-emitting relativistic jet outflow which also disappears after the plateau-ending X-ray/radio outburst

(see Klein-Wolt et al. (2002) for a detailed discussion). As also shown above, the IR flickering does not seem to correlate well with any particular X-ray variability from GRS 1915+105. The typical timescales for X-ray variability (e.g. the ~ 1 Hz QPO) are much less than the 8-second time resolution of the IR observations, and there is very little X-ray variability on these longer timescales – when smoothed to 8-second resolution, the X-ray lightcurve has an RMS of $\sim 3\%$ about a constant value. Thus, while there is significant activity in the inner accretion disk in GRS 1915+105 at this time, it is rather weak on the timescales seen in the IR. We conclude that it seems unlikely that the IR flickering arises from the accretion disk which is producing the jet. Rather, based on this apparent simultaneity of the plateau jet and the IR flickering, along with the lack of IR/X-ray correlation, it seems sensible to conclude that the enhanced IR emission of a few mJy arises from the quasi-continuous jet itself. Previous authors have also suggested that emission from the jet may enhance IR emission during the plateau state (Ueda, et al. (2002) ; Fuchs et al., (2003)).

Radio observations of this plateau jet indicate that the radio synchrotron emission begins in the optically thick regime, and the optical depth in the radio decreases to ~ 1 in the expanding jet at distances ~ 50 AU from the accretion disk and compact object (Klein-Wolt et al. (2002); Dhawan, et al. (2000)). If we assume that the opening angle of this jet is comparable to or larger than the large-scale jets observed from GRS 1915+105, then the diameter of the jet is ≥ 1 AU, or equivalently ~ 500 lt-s, at this distance. Given that the IR flickering occurs on timescales as fast as ~ 25 s (20 times faster than the light travel time across the jet diameter at $d \sim 50$ AU), we are forced to conclude that the IR flickering occurs much closer to the source of the jet itself – at a distance ≤ 2.5 AU.

We also note that the IR flux density excess seen here is $\sim 3 - 5$ mJy (compared to observations outside the plateau state), corresponding to $\sim 100 - 200$ mJy once we correct for the extinction towards GRS 1915+105 (Fender et al., (1997)). Assuming a distance of ~ 12 kpc for GRS 1915+105 (Mirabel & Rodríguez 1994), this gives an excess IR luminosity from the jet of $\nu L_\nu \sim 10^{36}$ ergs/s. This is much larger than the same number for the radio flux from the plateau jet ($\nu L_\nu \sim 10^{32}$ ergs/s), indicating that the IR jet luminosity dominates the radio jet luminosity by several orders of magnitude. The overall luminosity of the system at this stage, however, remains dominated by the X-ray flux from the inner accretion disks, at levels of $\sim 10^{38}$ ergs/s. Thus, the radiated power in the jet we observe here is $\sim 1\%$ of the total luminosity of GRS 1915+105.

4.3. What Drives the Fast IR Flickering?

If the rapid IR flickering, unlike the previously-reported Class B and Class C flares, does *not* arise in the inner accretion disk but the jet, we must consider the question, “What drives the rapid IR flickering on $\sim 30 - 60$ s timescales?”. Without the direct influence of the inner accretion disk, the most obvious possibility is that the timescales seen in the IR flickering are the natural timescales of some sort of instability in the jet itself, near its base. Several effects near the jet base are expected to generate shocks/instabilities. First of all, the actual jet base – the location where particles are initially accelerated away from the compact object – is expected to be a significant source of non-thermal radiation. While it is generally considered that the non-thermal X-ray emission from these systems (which is essentially *all* of the X-ray emission from GRS 1915+105 in the plateau state) may be the primary radiation from the particle acceleration process, it is not impossible that significant IR radiation arises here as well. Secondly (and perhaps more likely), there may be a jet collimation point, where the previously-accelerated outflow from the jet base is constrained to move with much smaller opening angles ($\sim 1^\circ$). Such behavior is predicted by several theoretical models for jet formation, and apparently confirmed by the radio observations of the M87 jet near its base (Junor, et al. 1999). If the jet base emission is in fact dominated by the non-thermal X-rays, the particles may have “cooled” enough at the collimation point to emit predominantly in the IR waveband. For either of these scenarios, further support may come from the fact that several authors have previously identified an “IR break” in the spectrum of the X-ray binary jet source GX 339-4 (Motch, et al. (1985); Corbel & Fender (2002); Nowak, et al. (2005)). In some models of jet formation this break is directly associated to the shock-acceleration region of the jet (Markoff et al. 2003) – applying this to GRS 1915+105 would naturally lead to the interpretation of the flickering observed here as coming from the jet launch region. Finally, jet outflows from supermassive black holes show clear evidence of internal shocks within the collimated jet flow even further “downstream” from the collimation point. If such shocks occur close enough to the compact object, they may also produce rapid IR flickering as seen here. Future observations of this flickering which could further constrain these possibilities should give key insights into the formation of the plateau jet in GRS 1915+105.

5. Conclusion

We have presented near-infrared observations of the microquasar GRS 1915+105 using the NICMOS instrument of the Hubble Space Telescope before, during, and after a “plateau” state in March-May 2003. During the X-ray/radio plateau, we find that the infrared flux is

significantly higher and more strongly variable than outside the plateau. In particular, we find “flickering” events with amplitudes $> 20\%$ occurring on e-folding timescales of ~ 30 s. These timescales are several times faster than any previously-observed infrared variability in GRS 1915+105, and do not seem to be correlated with any X-ray events of similar amplitude/timescale. As such, they seem to represent an entirely new mode of IR variability from GRS 1915+105. Based on the simultaneity of this flickering with the plateau jet and the lack of IR/X-ray correlation on the flickering timescales, we conclude that the IR flickering arises in the plateau jet itself. If so, the IR jet luminosity is much greater than the corresponding radio jet luminosity. Also, the IR flickering must occur very near the base of the jet (< 2.5 AU from the accretion disk). The lack of correlation with inner disk activity implies that $\sim 30 - 60$ s is a natural timescale of the jet at this range of locations, and that the flickering may be due to shocks at either the site of particle acceleration, the site of jet collimation, or internal shocks in the jet. Further study could give important insights into the formation of the plateau jet in GRS 1915+105.

The authors wish to thank the staff of the Space Telescope Science Institute, particularly, N. Schulz, for their help and support for this TOO program with NICMOS. The authors also thank the anonymous referee for helpful suggestions. SSE and SGP were supported in part by a STScI grant, by an NSF CAREER award (AST-0328522), and NSF grant AST-0507547. DMR was supported in part by a National Science Foundation Graduate Research Fellowship

REFERENCES

- Bandyopadhyay,R., et al. 1998, MNRAS, 295, 623
- Castro-Tirado,A., et al. 1994, ApJS, 92, 469
- Corbel.S. & Fender,R. 2002, ApJ, 573, L35
- Dhawan,V., Mirabel,I.F., Rodríguez,L.F. 2000, ApJ, 543, 373
- Eikenberry,S.S., Matthews,K., Morgan,E.H., Remillard,R.A., Nelson,R.W. 1998a, ApJ, 494, L61
- Eikenberry,S.S., Matthews,K., Murphy,T.W., Nelson,R., Morgan,E.H., Remillard,R.A., Munro,M. 1998b, ApJ, 506, L31
- Eikenberry,S.S., Matthews,K., Munro,M., Blanco,P.R., Morgan,E.H., Remillard,R.A. 2000, ApJ, 532, L33

- Eikenberry, S.S. & Fazio, G.G. 1997, *ApJ*, 475, L53
- Fender, R.P. et al. 1999, *MNRAS*, 304, 865
- Fender, R.P. & Pooley, G.G. 1998, *MNRAS*, 300, 573
- Fender, R.P., Pooley, G.G., Brocksopp, C., Newell, S.J. 1997, *MNRAS*, 290, L65
- Foster, et al. 1996, *ApJ*, 467, L81
- Fuchs, Y., Rodriguez, J., Mirabel, I.F., Chaty, S., Rib, M., Dhawan, V., Goldoni, P., Sizun, P., Pooley, G.G., Zdziarski, A.A., Hannikainen, D.C., Kretschmar, P., Cordier, B., Lund, N., *A&A*, 409, L35
- Jahoda, K., et al., 2006 *ApJS*, in press
- Junor, W., Biretta, J.A., Livio, M. 1999, *Nature*, 401, 891
- Klein-Wolt, M., Fender, R.P., Pooley, G.G., Belloni, T., Migliari, S., Morgan, E.H., van der Klis, M. 2002, *MNRAS*, 331, 745
- Levine, A. M., et al. 1996, *ApJ*, 469, L33
- Markoff, S., Nowak, M., Corbel, S., Fender, R., Falcke, H. 2003, *A&A*, 397, 645
- McClintock, J.E., & Remillard, R.A. 2006, in *Compact Stellar X-ray Sources*, eds. W.H.G Lewin & M. van der Klis, Cambridge: Cambridge University Press, pp.157–214; astro-ph/0306213
- Mikles, V., Eikenberry, S.S., Rothstein, D.M. 2006, *ApJ*, 637, 978
- Mirabel, I.F., Dhawan, V., Chaty, S., Rodriguez, L.F., Robinson, C., Swank, J., Geballe, T. 1998, *A&A*, 330, L9
- Mirabel, I.F. & Rodríguez, L.F. 1994, *Nature*, 371, 46
- Mirabel, I.F. & Rodríguez, L.F. 1999, *ARA&A*, 37, 409
- Mitsuda, K., Inoue, H., Koyama, K., Makishima, K., Matsuoka, M., Ogawara, Y., Shibazaki, N., Suzuki, K., Tanaka, Y., & Hirano, T. 1984, *PASJ*, 36, 741
- Motch, C., Ilovaisky, S.S., Chevalier, C., Angebault, P. 1985, *Space Sci Rev*, 40, 219
- Muno, M.P. et al. 2001, *ApJ*, 556, 515

- Muno, M. P., Morgan, E. H. & Remillard, R. A. 1999, *ApJ*, 527, 321
- Nowak, M.A., Wilms, J., Heins, S., Pooley, G., Pottschmidt, K. Corbel, S. 2005, *ApJ*, 626, 1006
- Pooley, G.G. & Fender, R.P. 1997, *MNRAS*, 292, 925
- Remillard, R.A. 2004, in *Procs., Texas@Stanford 2004*, ed., P. Chen, SLAC Electronic Conference Proceedings Archive; astro-ph/0504129
- Rothstein, D.M., Eikenberry, S.S., Matthews, K. 2005, *ApJ*, 626, 991
- Sams, B.J., Eckart, A., Sunyaev, R. 1996, *Nature*, 382, 47
- Thompson, R.I., Rieke, M., Schneider, G., Hines, D.C., Corbin, M.R. 1998, *ApJ*, 492, L95
- Ueda, Y., Yamaoka, K., Snchez-Fernndez, C., Dhawan, V., Chaty, S., Grove, J.E., McCollough, M., Castro-Tirado, A.J., Mirabel, F., Kohno, K., Feroci, M., Casella, P., Trushkin, S.A., Castaneda, H., Rodrguez, J., Durouchoux, P., Ebisawa, K., Kotani, T., Swank, J., Inoue, H. 2002, *ApJ*, 571, 918

Table 1.

Visit	Date (MJD)	F187W mean flux density (mJy)	Excess Variability (% RMS) ^a
1	52736.60290	2.54	1.0
2	52741.67225	6.28	6.9
3	52746.87292	4.24	4.8
4	52752.87847	5.10	7.8
5	52763.68303	3.66	4.0
6	52796.43359	2.41	0.8
7	52801.71115	2.11	< 2.0
8	52808.31191	2.26	1.8
9	52814.71761	2.31	< 2.0

^aExcess variability RMS % is defined as $\sqrt{\sigma_{sample}^2 - \sigma_{meas}^2}/mean$ where σ_{sample} is the RMS scatter in the sample values, σ_{meas} is the pipeline-estimated measurement noise RMS, and $mean$ is the mean value of the sample points. Values reported as < 2.0 % indicate that the RMS sample scatter is less than the estimated RMS measurement noise, and we take σ_{meas} as an upper limit on σ_{sample} .

Table 2.

Visit	Filter	Date (MJD)	UT (s)	Characteristic Rise Time (s)	Upper Limit (s)
2	F187W	52741	58234	58 ± 8	71
2	POL0L	52741	59079	31 ± 4	38
2	POL120L	52741	59483	43 ± 7	55
3	F187W	52746	75663	27 ± 9	50
3	F187W	52746	75691	49 ± 7	61
3	F187W	52746	75818	64 ± 13	88
3	POL120L	52746	76755	52 ± 9	70
4	F187W	52752	75904	28 ± 9	48
4	F187W	52752	76289	45 ± 5	54
4	F187W	52752	76392	55 ± 6	65
4	POL0L	52752	76529	51 ± 9	69
4	POL0L	52752	76735	48 ± 9	65
4	POL120L	52752	77163	30 ± 4	37
4	POL240L	52752	77369	28 ± 3	34
4	POL240L	52752	77654	37 ± 5	45

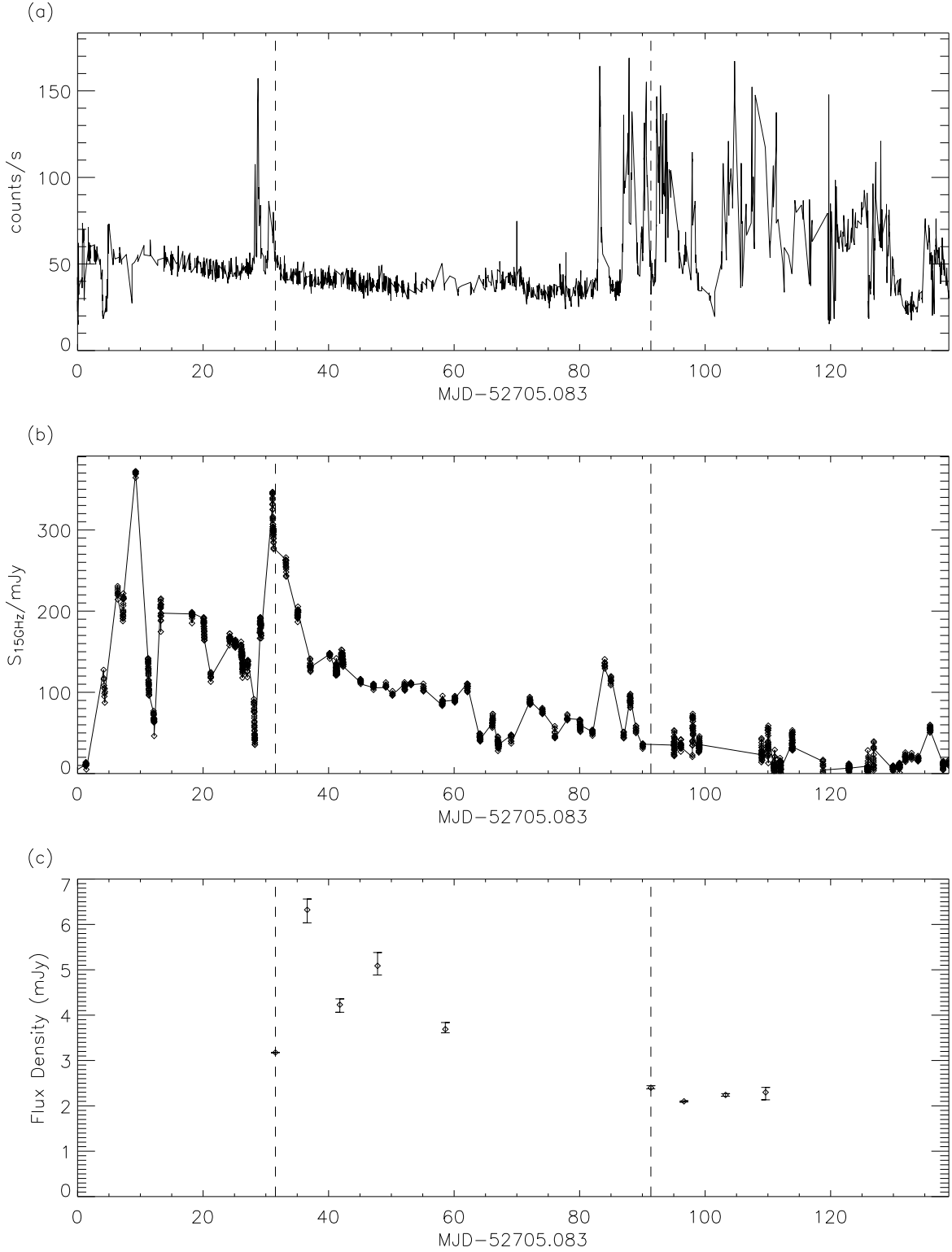


Fig. 1.— Multiwavelength light curves of GRS 1915+105. (Top) X-ray lightcurve from the RXTE ASM. (Middle) Radio lightcurve from the Ryle Telescope. (Bottom) Near-infrared (1.87 μm) lightcurve from *HST/NICMOS*. For the near-IR lightcurve, note that the bars indicate the *range* of the variable flux density values during each observation, rather than the uncertainties. Vertical lines provide a time reference for comparison among the different

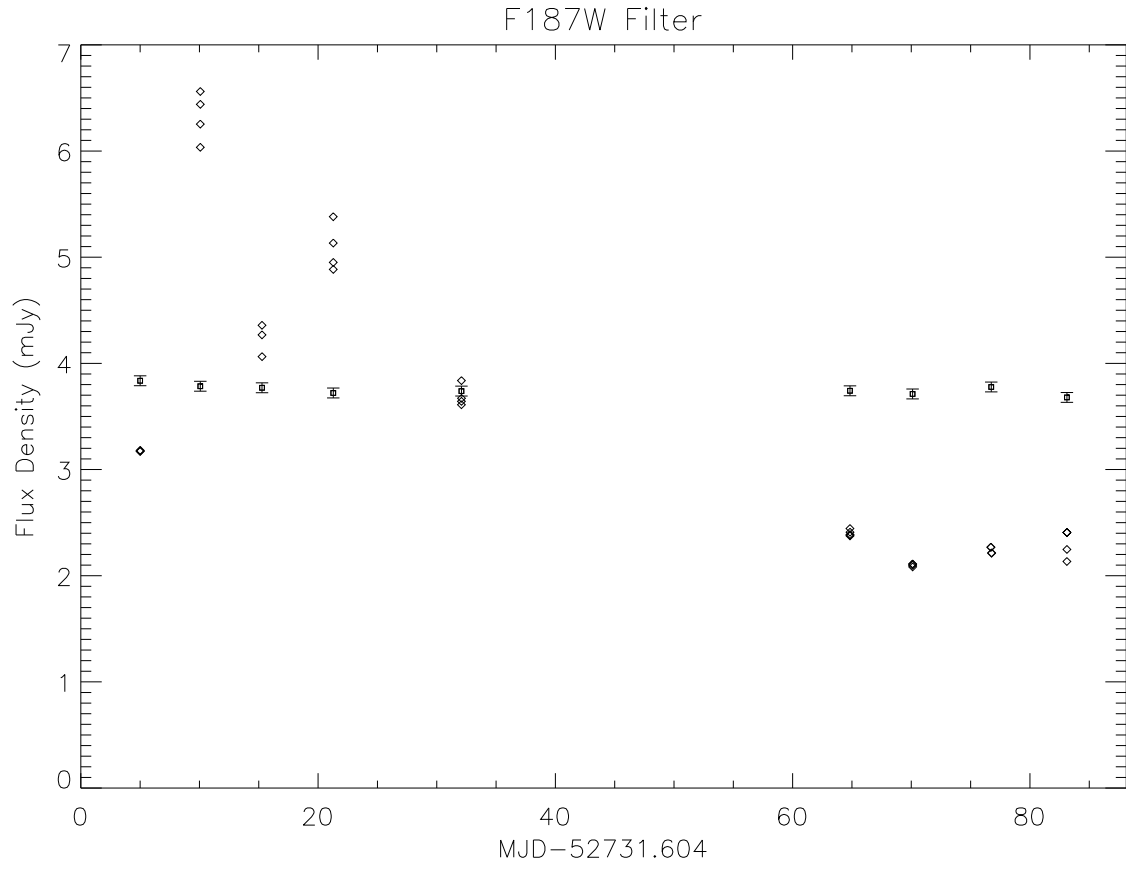


Fig. 2.— Flux densities for GRS 1915+105 (Diamonds) and Star A (Squares) in NICMOS F187W filter. Note that Star A, which has similar brightness to GRS 1915+105, is quite steady while GRS 1915+105 varies both between visits and within individual visits.

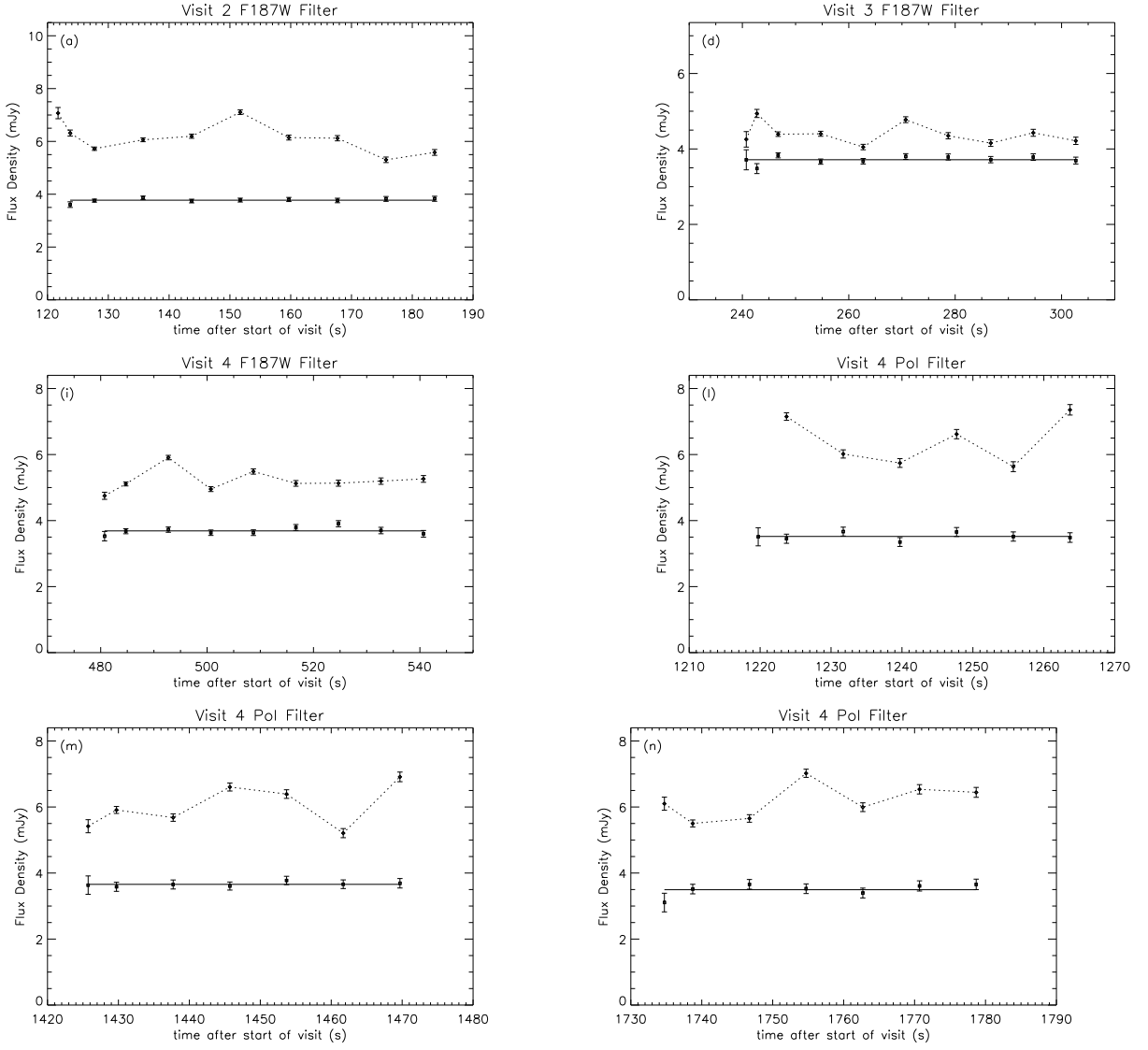


Fig. 3.— Selected high time-resolution near-IR lightcurves for GRS 1915+105.

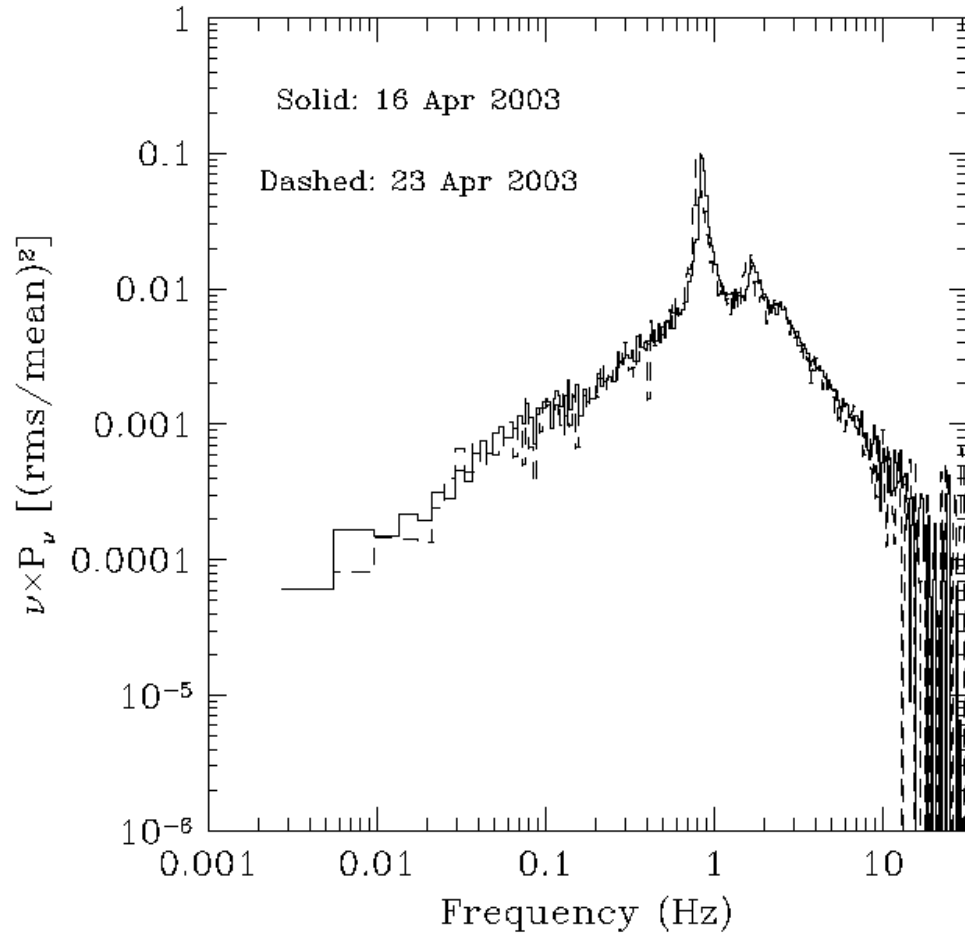


Fig. 4.— X-ray power density spectra of GRS 1915+105 for 16 April 2003 (solid) and 23 April 2003 (dash).